ORIGINAL PAPER

MHD STAGNATION POINT FLOW OF HYPERBOLIC TANGENT FLUID WITH VISCOUS DISSIPATION AND CHEMICAL REACTION

KINZA ARSHAD[1], MUHAMMAD ASHRAF[1]

Manuscript received: 26.08.2020; Accepted paper: 10.03.2021;
Published online: 30.06.2021.

Abstract. *In the present work, two dimensional flow of a hyperbolic tangent fluid with chemical reaction and viscous dissipation near a stagnation point is discussed numerically. The analysis is performed in the presence of magnetic field. The governing partial differential equations are converted into non-linear ordinary differential equations by using appropriate transformation. The resulting higher order non-linear ordinary differential equations are discretized by finite difference method and then solved by SOR (Successive over Relaxation parameter) method. The impact of the relevant parameters is scrutinized by plotting graphs and discussed in details. The main conclusion is that the large value of magnetic field parameter and wiessenberg numbers decrease the streamwise and normal velocity while increase the temperature distribution. Also higher value of the Eckert number Ec results in increases in temperature profile.*

Keywords: *Hyperbolic tangent fluid; viscous dissipation; magnetic field; chemical reaction.*

1. INTRODUCTION

Flows over stretching surfaces have been attaining the great importance for many decades due to their wide applications in industry and engineering such as glass fiber, metal spinning, paper production, wires drawing etc. In this direction Basha et al. [1] studied effect of hall and ion-split on MHD steady flow through a porous medium in a vertical microchannel with free convective conditions. Khan and Pop [2] investigated numerically the boundary layer flow of a nanofluid over a stretching sheet. Nazar et al. [3] deliberated the boundary layer unsteady flow due to a stretching sheet in a rotating fluid. Viscous flow analysis due to stretching sheet with suction and slip was elaborated by Wang [4]. Rana and Bhargava [5] examined laminar boundary layer flow and heat transfer of a nanofluid over a nonlinear stretching sheet. Cattaneo-Christov heat flux model for viscoelastic flow due to an exponentially stretching surface was numerically studied by Khan et al. [6]. Viscous dissipation and radiation effect on a thermal boundary layer flow over a non-linearly stretching sheet was explored by Cortell [7]. Pramanik [8] analyzed the flow and heat transfer of Casson fluid over an exponentially porous stretching surface with thermal radiation

The study of stagnation point flow has a countless prominence in arena of fluid mechanics. It has engrossed great attention of researchers during the past few eras. For-instance, Ashraf and Ashraf [9] calculated stagnation point flow of a micropolar fluid on a heated surface in the presence of magnetic field. Shah et al. [10] examined the variable thermal conductivity impact on stagnation point boundary layer flow over a Riga plate with

[1] Bahauddin Zakariya University, Centre for Advanced Studies in Pure and Applied Mathematics (CASPAM), 60800 Multan, Pakistan. E-mail: kinzaarshad61@yahoo.com; muhammadashraf@bzu.edu.pk.

variable thickness via generalized Fourier's law. Mustafa et al. [11] presented the analytic solution of stagnation point flow of a nanofluid towards a stretching sheet. He also examined the effects of Brownian motion and thermophoresis on the flow. Furthermore, mixed convection non-axisymmetric Homann stagnation point flow was investigated by Lok et al. [12].

Magnetohydrodynamic flows have revealed abundant interest of many researchers owing to their frequent real world applications like in magnetic wound or cancer tumor cure causing hypothermia, cooling of fission reaction, magnetic endoscopy, bleeding reduction throughout surgeries etc. Moreover, many technological problems are also subjected to MHD analysis. For example: in the designing of heat exchangers, in thermal protection and in vehicle propulsion. Khan et al. [13] analyzed numerically MHD Carreau fluid flow past a stretching cylinder with homogenous-heterogeneous reactions. Ashraf and Batool [14] analyzed MHD micropolar fluid over a stretchable disk with heat transfer effects. Mohyud-Din et al. [15] considered a study of heat and mass transfer on MHD flow of nanoparticles. Sulochana et al. [16] scrutinized numerically the MHD radiative flow over a rotating cone in the presence of Soret and chemical reaction. Multiple Analytic Solutions of Heat and Mass Transfer of Magnetohydrodynamic Slip Flow for Two Types of Viscoelastic Fluids past a Stretching Sheet was analyzed by Turkyilmazoglu [17]. Sandeep et al [18] studied the unsteady radiative MHD flow and heat transfer characteristics of a dusty nanofluid past an exponentially stretching surface Baag et al. [19] studied entropy generation for viscoelastic MHD flow over a stretching sheet entrenched in a porous medium. Hayat et al. [20] explored MHD flow of Jeffery fluid with heat source and power law and heat flux. Turkyilmazoglu et al. [21] studied unsteady rear stagnation-point flow past off-centered deformable surfaces with magnetic field effects.

In recent times, substantial attention has been paid on hyperbolic tangent fluid for the reason that it has numerous engineering and industrial applications, such as food mixing, multigrade oil, plasma and composite materials. Basically, it is a non-Newtonian fluid model, which measures the fluid resistance when the increment in shear stress causes decrement in flow. Common examples encompass blood, paint, ketchup, whipped cream and nail polish. Kumar et al. [22] studied an unsteady squeezed flow of a tangent hyperbolic fluid over a sensor surface in the presence of variable thermal conductivity. Nadeem and Akram [23] discussed the partial slip effects on the peristaltic transport of a tangent hyperbolic fluid model in an asymmetric channel. Nadeem and Shahzadi [24] scrutinized the inspiration of induced magnetic field on nano hyperbolic tangent fluid in a curved channel. Akbar et al. [25] investigated mass and heat transfer effects on peristaltic flow of a tangent hyperbolic fluid in an annulus. Iqbal et al. [26] examined the influence of Cattaneo-Christov heat flux modeled on MHD hyperbolic tangent fluid over a moving porous surface. Akbar et al. [27] investigated numerically MHD boundary layer flow of tangent hyperbolic fluid past a stretching sheet by using fourth and fifth order Runge–Kutta–Fehlberg method. Hayat et al. [28] presented Peristaltic transport of tangent hyperbolic fluid with variable viscosity. Abbas et al. [29] described the three dimensional peristaltic flow of hyperbolic tangent fluid in nonuniform channel having flexible walls. Salahuddin et al. [30] analyzed the tangent hyperbolic nanofluid impinging on a stretching cylinder near the stagnation point.

Flow with heat and mass transfer and chemical reaction is quite noticeable in a number of processes. Such processes are well-known in a chemical industry, cooling of nuclear reactors and petroleum industries. Chemical reactions are classified as either homogeneous or heterogeneous processes. In homogeneous process, reaction occurs uniformly throughout a given phase. A heterogeneous reaction is the one that takes place in a restricted area or within the boundary of the phase. Hayat et al. [31] examined the effect of

thermal radiation in a mixed convective flow of a tangent hyperbolic fluid employed by convective conditions and chemical reaction.

Various investigators have taken the consideration in viscous dissipation in fluids nowadays. For instance Khan et al. [32] discussed modified homogeneous-heterogeneous reactions for MHD stagnation flow with viscous dissipation and Joule heating. Motsumi and Makinde [33] analyzed the effects of thermal radiation and viscous dissipation on boundary layer flow of nanofluid over a permeable moving flat plate. Bataller [34] studied viscoelastic fluid flow and heat transfer over a stretching sheet under the effects of a non-uniform heat source, viscous dissipation and thermal radiation. Kumar et al. [35] examined effect of viscous dissipation on MHD flow of micropolar fluid past a stretching surface with modified heat flux model. Moreover, MHD natural convection in saturated porous media in the presence of thermal radiation and heat generation/absorption was investigated by Turkyilmazoglu [36]. Khan et al. [37] discussed radiative flow of hyperbolic tangent fluid having double stratification under the influence of chemical reaction with convective condition.

In the present article, we consider two dimensional magnetohydrodynamic stagnation point flow of a hyperbolic tangent fluid with viscous dissipation and chemical reaction. The modeled equations are converted into ordinary nonlinear equations which are then solved numerically by SOR method. The effect of physical parameters of interest are presented and discussed.

2. MATERIALS AND METHODS

2.1. MATERIALS

We deliberate the steady, incompressible MHD flow of tangent hyperbolic fluid over a stretching sheet taking into account the thermal radiation, viscous dissipation and chemical reaction effects near a stagnation point. The fluid motion is generated due to stretching of the sheet. The stretching velocity of the sheet is $u_w(x) = ax$ whereas the velocity of the external flow is $u_e(x) = cx$, where a and c are positive constants.By following [31], magnetic field of strength B^2 is applied normal to the surface of sheet. Additionally, the temperature equation is assumed with the effects of viscous dissipation term $\mu\left(\frac{\partial u}{\partial y}\right)^2$ .The governing boundary layer equations of conservation, linear momentum, heat and concentration for the present problem are [31]:

$$\frac{\partial u}{\partial x}+\frac{\partial v}{\partial y}=0 \tag{1}$$

$$u\frac{\partial u}{\partial x}+v\frac{\partial v}{\partial y}=u_e\frac{du_e}{dx}+\nu(1-n)\frac{\partial^2 u}{\partial y^2}+\sqrt{2}\nu\Gamma n\frac{\partial u}{\partial y}\frac{\partial^2 u}{\partial y^2}+\frac{\sigma B^2}{\rho}(u_e-u) \tag{2}$$

$$\rho c_p\left(u\frac{\partial T}{\partial x}+v\frac{\partial T}{\partial y}\right)=k\frac{\partial^2 T}{\partial y^2}+\mu\left(\frac{\partial u}{\partial y}\right)^2 \tag{3}$$

$$u\frac{\partial C}{\partial x}+v\frac{\partial C}{\partial y}=D\frac{\partial^2 C}{\partial y^2}-k_1(C-C_\infty) \tag{4}$$

The boundary conditions for the flow, heat and concentration analysis are [31]

$$\begin{aligned} &u=u_w(x)=ax,\ v=0,\ T=T_w,\ C=C_w \ at\ y=0,\\ &u=u_e(x)=cx,\ \ T\to T_\infty,\ \ C\to C_\infty\ \ as\ \ y\to\infty. \end{aligned} \tag{5}$$

Here u and v are the respective velocity components in the x- and y-direction, n is the power law index, $\nu=(\mu/\rho)$ is the kinematic viscosity, ρ is the density , Γ is the Williamson parameter, c_p is the specific heat at constant pressure, k_1 is the reaction rate, D is the mass diffusivity, $u_w(x)$ is the linear stretching velocity, T and C are the fluid temperature and concentration, respectively, $u_e(x)$ is the free stream velocities, c is the rate of free stream velocity and a is the stretching rate.

Taking the following similarity transformations [31]

$$\begin{aligned} &\eta=y\sqrt{\frac{a}{\nu}},\ \ \theta(\eta)=\frac{T-T_\infty}{T_f-T_\infty},\ \ G(\eta)=\frac{C-C_\infty}{C_f-C_\infty},\\ &\psi(\eta)=x\sqrt{a\nu}F(\eta),\ u=xaF'(\eta),\ v=-\sqrt{a\nu}F(\eta), \end{aligned} \tag{6}$$

Equation (1) is identically satisfied and eqs. (2),(3), (4) and (5) are reduced to

$$(1-n)F'''-F'^2+FF''+nWeF'''(F'')+Aa^2+M(Aa-F')=0, \tag{7}$$

$$\theta''+\Pr F\theta'+\Pr EcF''=0, \tag{8}$$

$$G''+ScfG'-Sc\gamma G=0, \tag{9}$$

$$\begin{aligned} &F(\eta)=0,\ \ F'(\eta)=1,\ \theta(0)=1\ G(0)=1\ at\ \eta=0,\\ &F'(\eta)=Aa,\quad \theta(\eta)=0,\quad G(\eta)=0\ as\ \eta\to\infty \end{aligned} \tag{10}$$

where We is the Weissenberg number, Aa is the ratio of rates or velocity ratio, $\Pr$ is the Prandtl number, Ec is the Eckert number, Sc is the Schmidt number, γ is the chemical reaction parameter.

These parameters are defined as follows:

$$We=\frac{\sqrt{2}a^{3/2}x\Gamma}{\sqrt{\nu}},\quad Aa=\frac{c}{a},\quad M=\frac{\sigma B^2}{a\rho}$$
$$Ec=\frac{a^2x^2}{\mu\left(T_w-T_\infty\right)},\ \mathrm{Pr}=\frac{\mu c_p}{k},\ Sc=\frac{\nu}{D},\ \gamma=\frac{k_1}{a}. \tag{11}$$

The skin friction coefficient, local Nusselt and Sherwood number are defined as

$$C_{f_\infty}=\frac{\tau_w}{\frac{1}{2}\rho u_w^2},\quad Nu_x=\frac{xq_w}{k(T_f-T_\infty)},\quad Sh_x=\frac{xj_w}{D(C_f-C_\infty)},$$

$$j_w=-D\left(\frac{\partial C}{\partial y}\right)_{y=0},\quad \tau_w=\left[(1-n)\frac{\partial u}{\partial y}+\frac{n\Gamma}{\sqrt{2}}\left(\frac{\partial u}{\partial y}\right)^2\right]_{y=0},$$

$$q_w=-k\left(\frac{\partial T}{\partial y}\right)_{y=0} \tag{12}$$

The skin friction coefficient C_{f_∞}, local Nusselt Nu_x and Sherwood number Sh_x in dimensionless form are given by means of

$$\mathrm{Re}_x^{1/2}C_{f_\infty}=(1-n)F''(0)+\frac{n}{2}We(F''(0))^2, \tag{13}$$

$$\mathrm{Re}_x^{-1/2}Nu_x=-\theta'(0), \tag{14}$$

$$\mathrm{Re}_x^{-1/2}Sh_x=-G'(0) \tag{15}$$

Here $\mathrm{Re}_x=\frac{u_w x}{\nu}$ denotes the local Reynolds number.

2.2. METHODS

We solve the equations (7), (8), (9) and (10) by SOR method. Primarily, we discretize these equations by applying finite difference method and then applied the successive over relaxation (SOR) method.

2.2.1. Finite difference method

To begin with, we reduce the order of equation (7) by means of reduction of order method. Putting $F_i'=q_i,\quad F_i''=q_i',\ F_i'''=q_i''$ in equation (7), we arrive at

$$(1-n)q_i''-q_i^2+F_iq_i'+nWeq_i''q_i'+Aa^2+M(Aa-q_i)=0 \tag{16}$$

Using the finite difference approximations, let

$$q_i' \approx \frac{q_{i+1}-q_{i-1}}{2h} \text{ and } q_i'' \approx \frac{q_{i+1}+q_{i-1}-2q_i}{h^2}$$

then equation (16) gives

$$(1-n)\left(\frac{q_{i+1}+q_{i-1}-2q_i}{h^2}\right)-q_i^{\,2}+F_i\left(\frac{q_{i+1}-q_{i-1}}{2h}\right)+nWe\left(\frac{q_{i+1}+q_{i-1}-2q_i}{h^2}\right)\left(\frac{q_{i+1}-q_{i-1}}{2h}\right)+Aa^2+M(Aa-q_i)=0 \tag{17}$$

or

$$q_i=\frac{Cq_{i+1}+Bq_{i-1}+D}{A}$$

where

$$A=\left(\frac{2(1-n)}{h^2}+\left(\frac{nWe}{h^3}\right)q_{i-1}-\left(\frac{nWe}{h^3}\right)q_{i+1}+M-q_i\right)$$

$$B=\left(\frac{(1-n)}{h^2}-\frac{F_i}{2h}-\left(\frac{nWe}{2h^3}\right)q_{i-1}\right)$$

$$C=\left(\frac{(1-n)}{h^2}+\frac{F_i}{2h}+\left(\frac{nWe}{2h^3}\right)q_{i+1}\right),\quad D=Aa^2+MAa.$$

Similarly for heat equation (8), letting

$\theta_i' \approx \frac{\theta_{i+1}-\theta_{i-1}}{2h}$ and $\theta_i'' \approx \frac{\theta_{i+1}+\theta_{i-1}-2\theta_i}{h^2}$, we obtain

$$\theta_i=\frac{C\theta_{i+1}+B\theta_{i-1}+D}{A} \tag{18}$$

Where

$$A=4h^2,\quad B=2h^2-h^3\,\mathrm{Pr}\,f_i,$$
$$C=2h^2+h^3\,\mathrm{Pr}\,f_i,$$
$$D=4\,\mathrm{Pr}\,Ec\left(q_{i+1}+q_{i-1}-2q_i\right)^2$$

For concentration equation (9), we have

$$G_i=\frac{CG_{i+1}+BG_{i-1}}{A} \tag{19}$$

Where

$$A=\left(\frac{2}{h^2}+Sc\gamma\right),\quad B=\left(\frac{1}{h^2}-\frac{ScF_i}{2h}\right),\quad C=\left(\frac{1}{h^2}+\frac{ScF_i}{2h}\right)..$$

3. RESULTS AND DISCUSSION

In this section the influence of dimensionless flow parameters precisely, the power-law index n, the ratio of rates Aa, Weissenberg number We, the magnetic parameter M, the radiation parameter Rd, the Prandtl number Pr, the chemical reaction parameter γ and the Eckert number Ec on the velocity, temperature and concentration field is discussed.

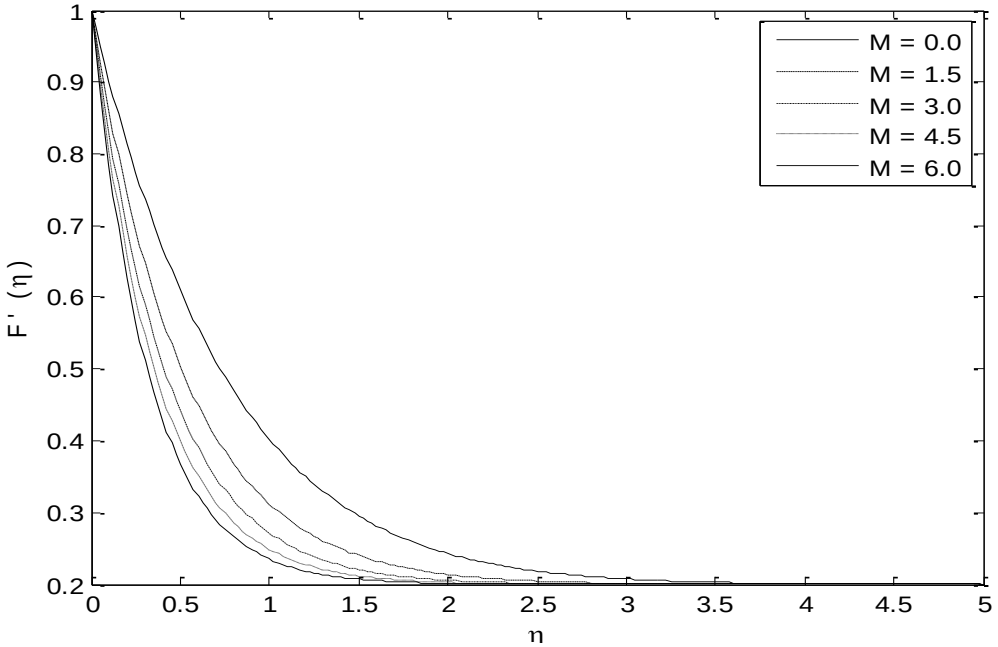

Figure 1. $F'(\eta)$ **for** $n = 0.2, We = 0.2, Aa = 0.2, Ec = 0.5, Pr = 0.5, Sc = 0.5, \gamma = 0.5$ **and various** M

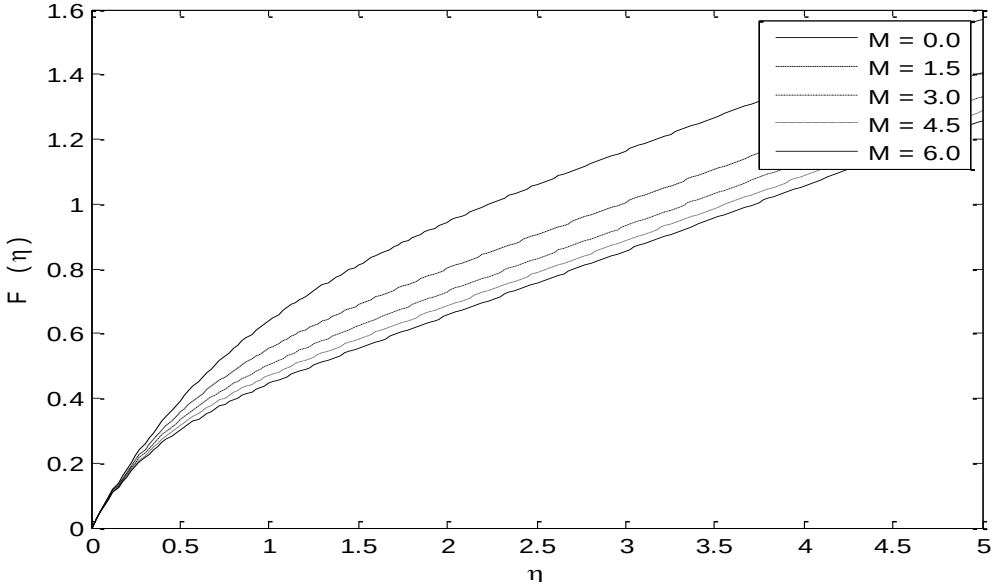

Figure 2. $F(\eta)$ **for** $n = 0.2, We = 0.2, Aa = 0.2, Ec = 0.5, Pr = 0.5, Sc = 0.5, \gamma = 0.5$ **and various** M

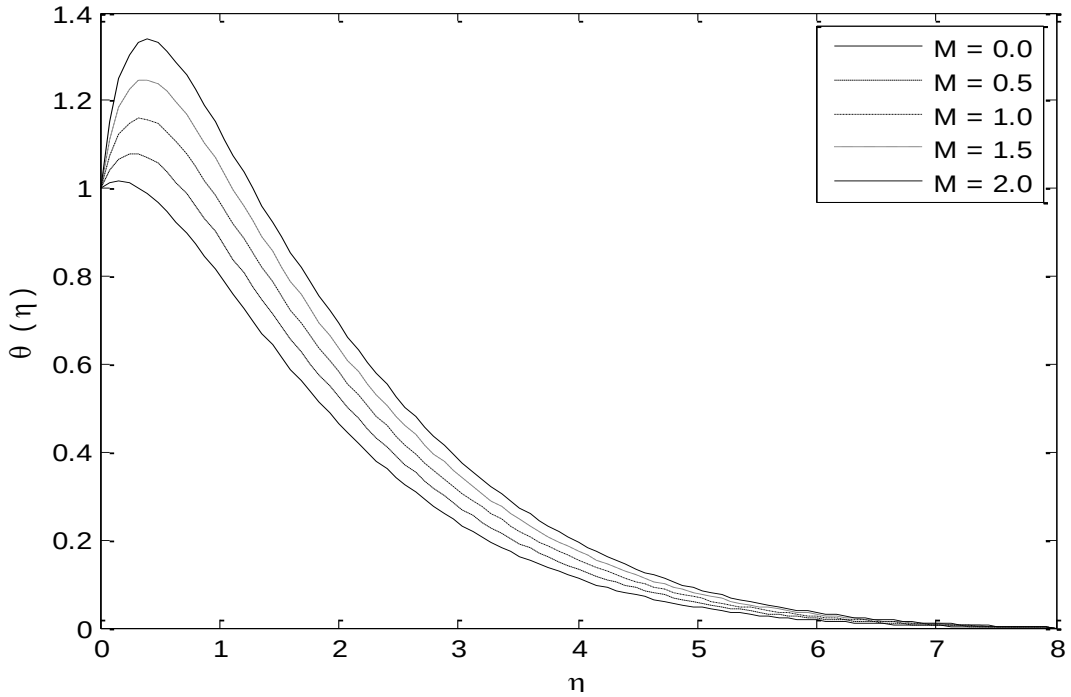

Figure 3. $\theta(\eta)$ **for** $n = 0.2, We = 0.2, Aa = 0.2, Ec = 0.5, Pr = 0.5, Sc = 0.5, \gamma = 0.5$ **and various** M

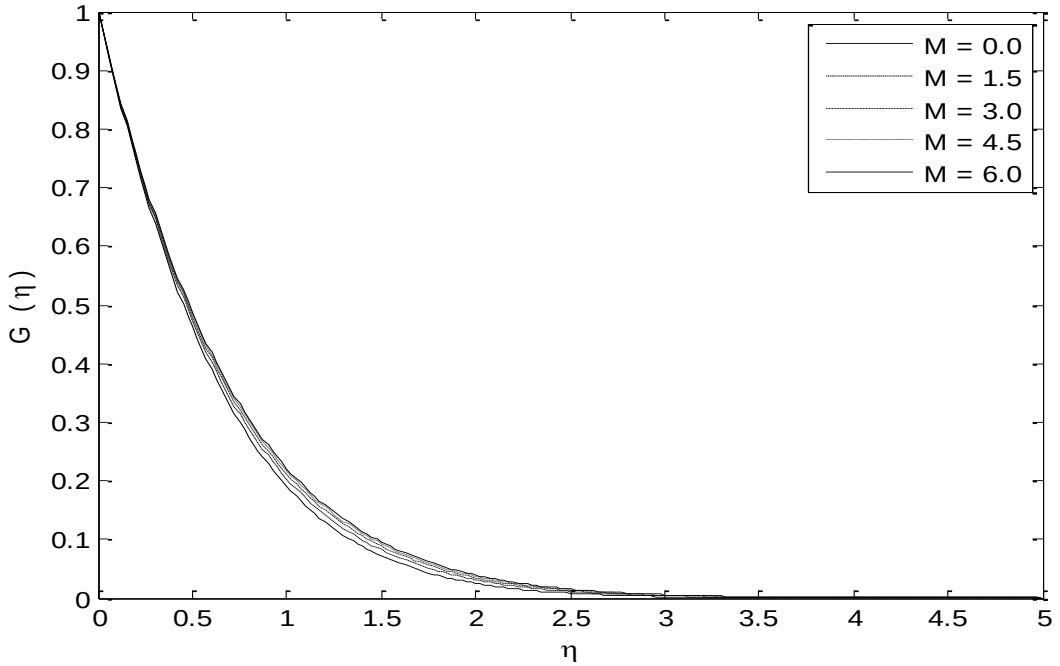

Figure 4. $G(\eta)$ **for** $n = 0.2, We = 0.2, Aa = 0.2, Ec = 0.5, Pr = 0.5, Sc = 0.5, \gamma = 0.5$ **and various** M

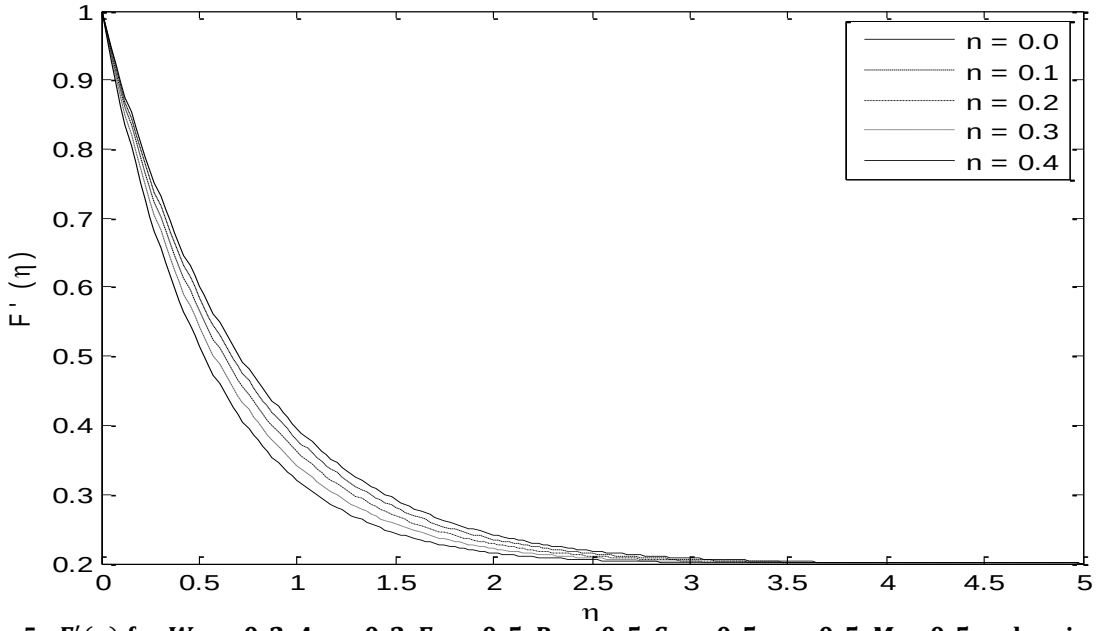

Figure 5. $F'(\eta)$ **for** $We = 0.2, Aa = 0.2, Ec = 0.5, Pr = 0.5, Sc = 0.5, \gamma = 0.5, M = 0.5$ **and various** n**.**

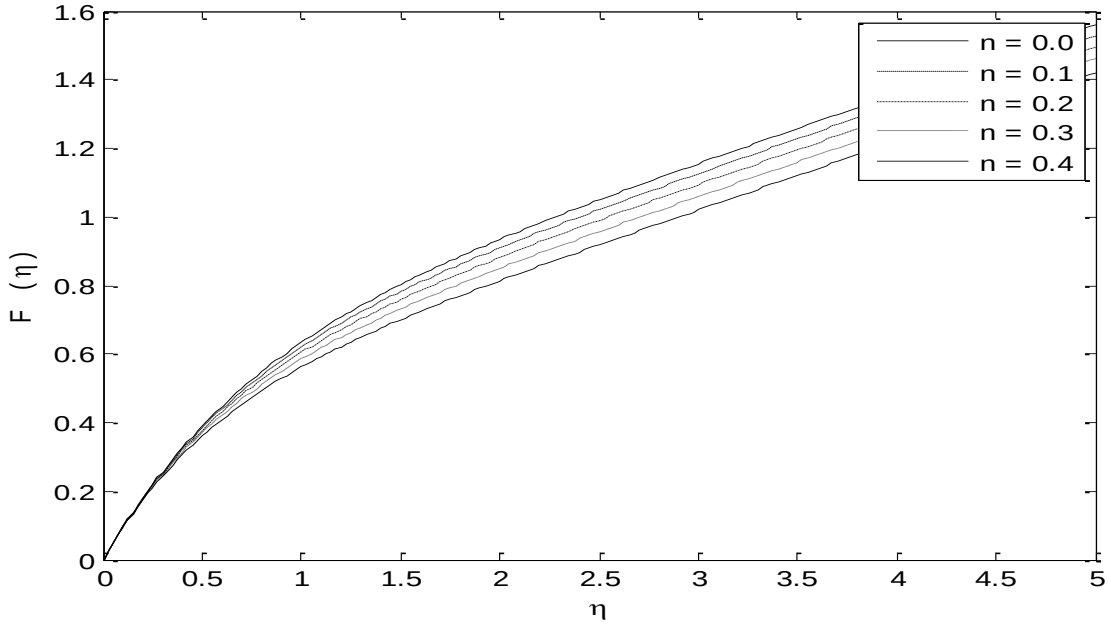

Figure 6. $F(\eta)$ **for** $We = 0.2, Aa = 0.2, Ec = 0.5, Pr = 0.5, Sc = 0.5, \gamma = 0.5, M = 0.5$ **and various** n**.**

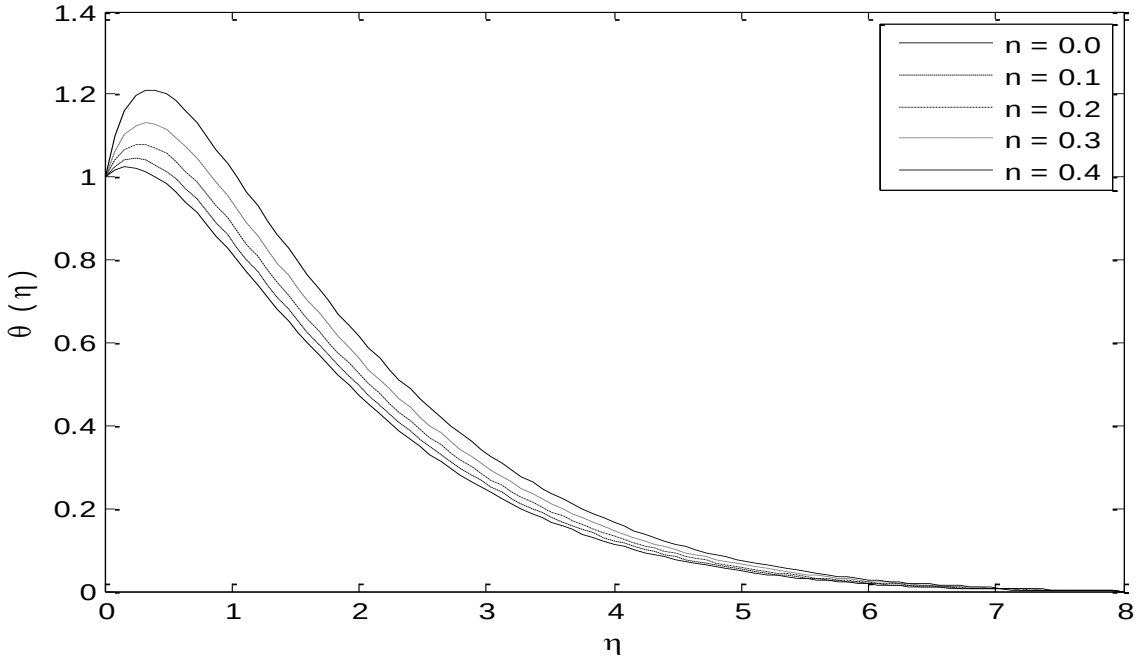

Figure 7. $\boldsymbol{\theta(\eta)}$ **for** $\boldsymbol{We = 0.2, Aa = 0.2, Ec = 0.5, Pr = 0.5, Sc = 0.5, \gamma = 0.5, M = 0.5}$ **and various** $\boldsymbol{n}$**.**

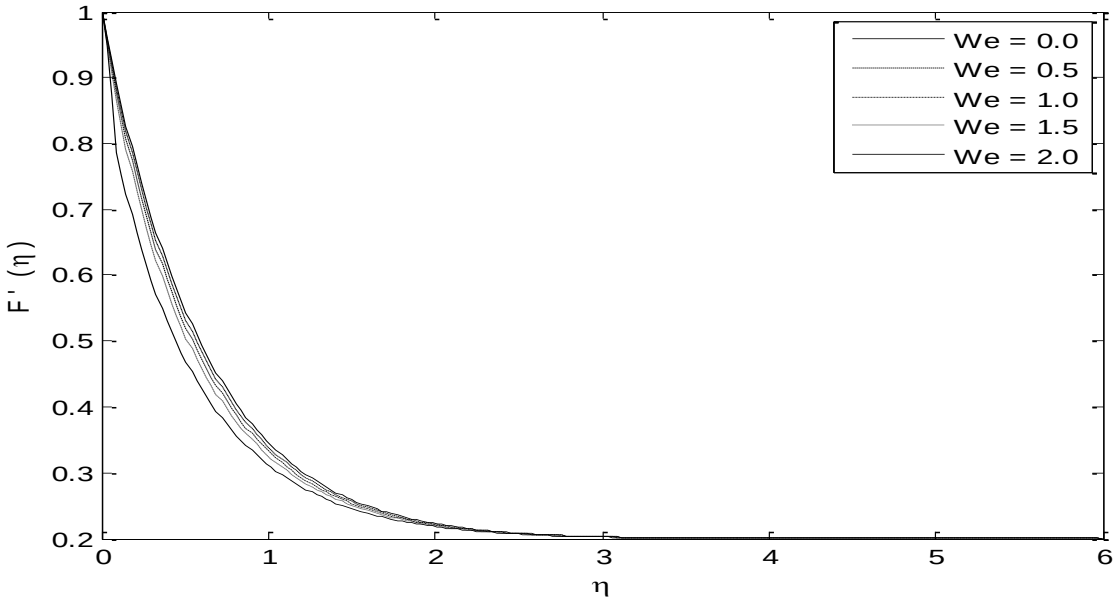

Figure 8. $\boldsymbol{F'(\eta)}$ **for** $\boldsymbol{n = 0.2, Aa = 0.2, Ec = 0.5, Pr = 0.5, Sc = 0.5, \gamma = 0.5, M = 0.5}$ **and various** $\boldsymbol{We}$

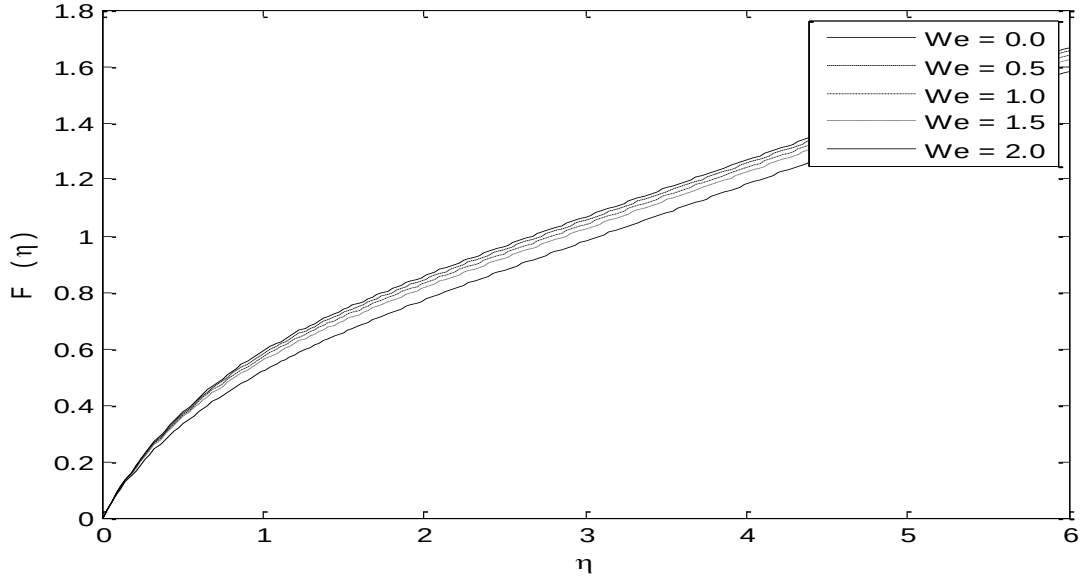

Figure 9. $F(\eta)$ **for** $n = 0.2, Aa = 0.2, Ec = 1.0, Pr = 0.5, Sc = 0.5, \gamma = 0.5, M = 0.5$ **and various** We

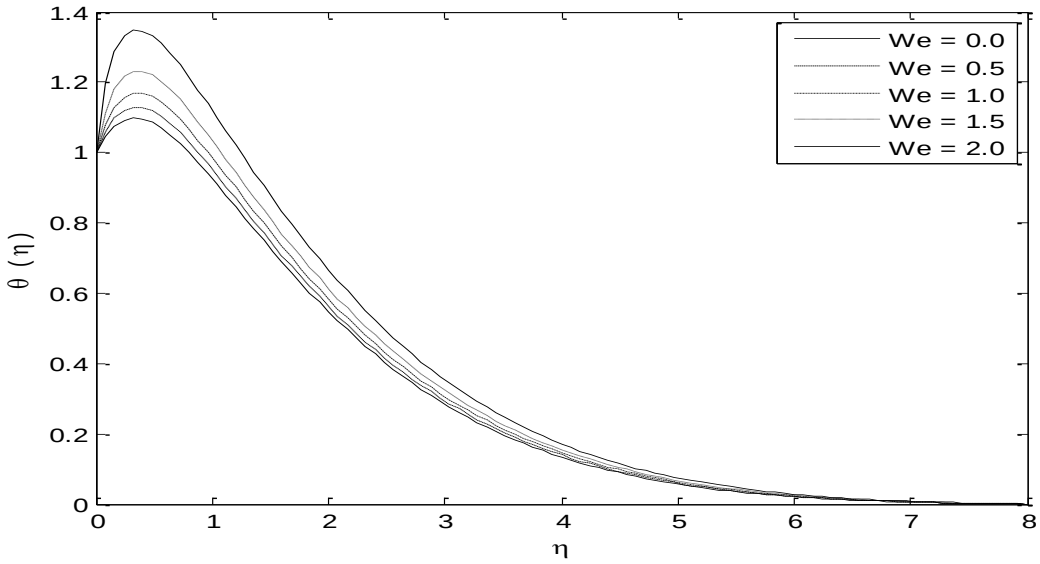

Figure 10. $\theta(\eta)$ **for** $n = 0.2, Aa = 0.2, Ec = 1.0, Pr = 0.5, Sc = 0.5, \gamma = 0.5, M = 0.5$ **and various** We**.**

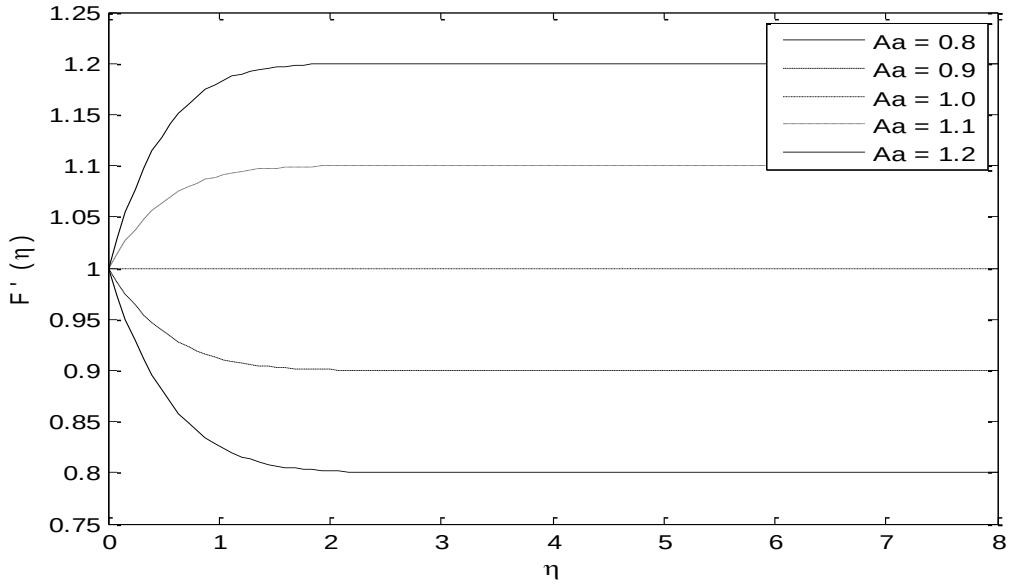

Figure 11. $F'(\eta)$ **for** $n = 0.2, We = 0.2, Ec = 1.0, Pr = 0.5, Sc = 0.5, \gamma = 0.9, M = 0.2$ **and various Aa**

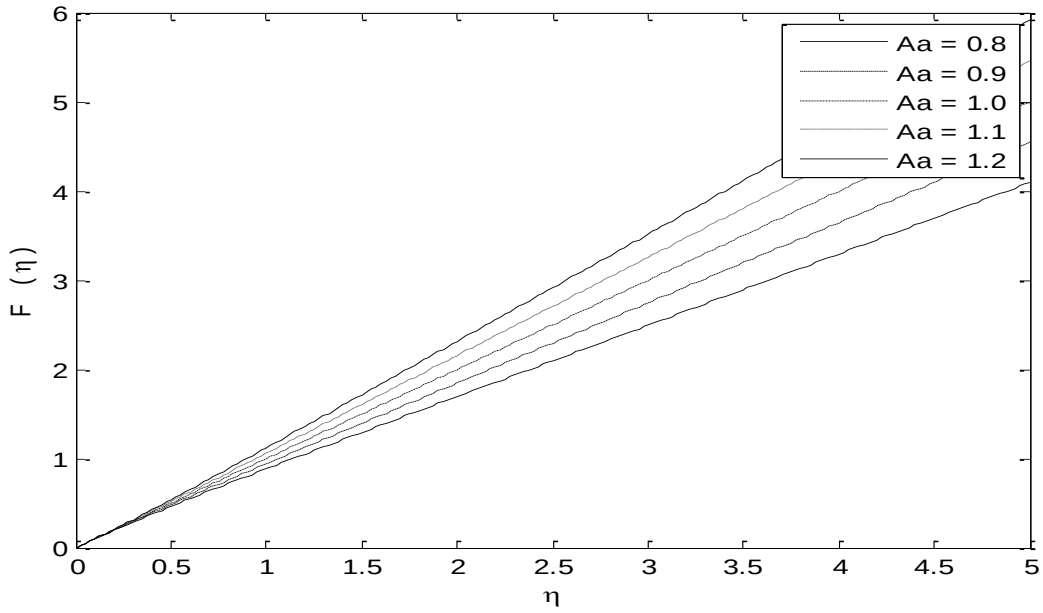

Figure 12. $F(\eta)$ **for** $n = 0.2, We = 0.2, Ec = 1.0, Pr = 0.5, Sc = 0.5, \gamma = 0.9, M = 0.2$ **and various** Aa

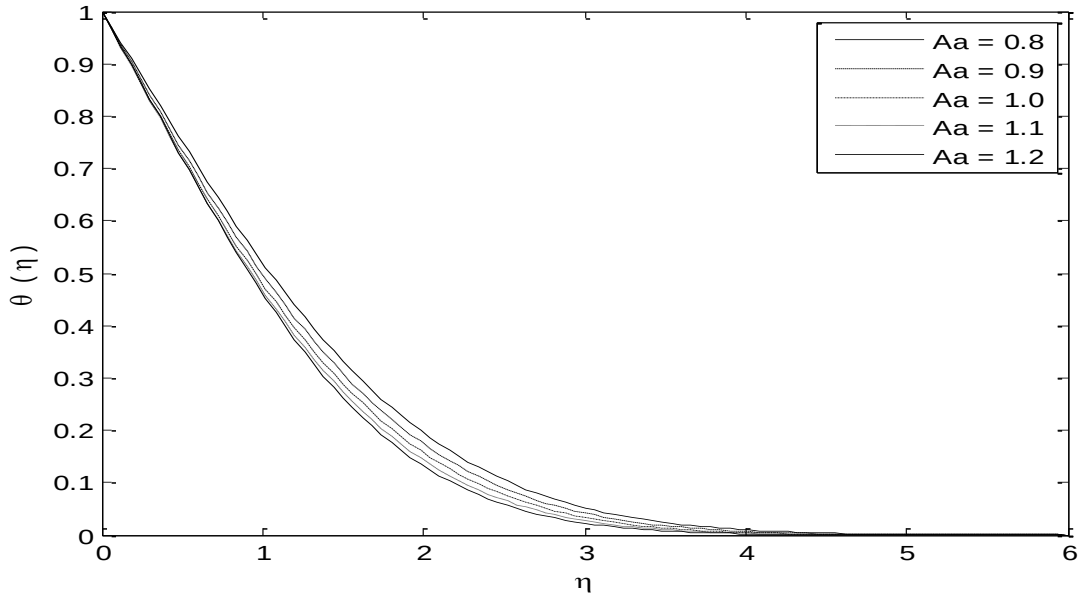

Figure 13. $\theta(\eta)$ **for** $n = 0.2, We = 0.2, Ec = 1.0, \gamma = 0.5,\ Sc = 0.5, Pr = 0.5, M = 0.2$ **and various** Aa

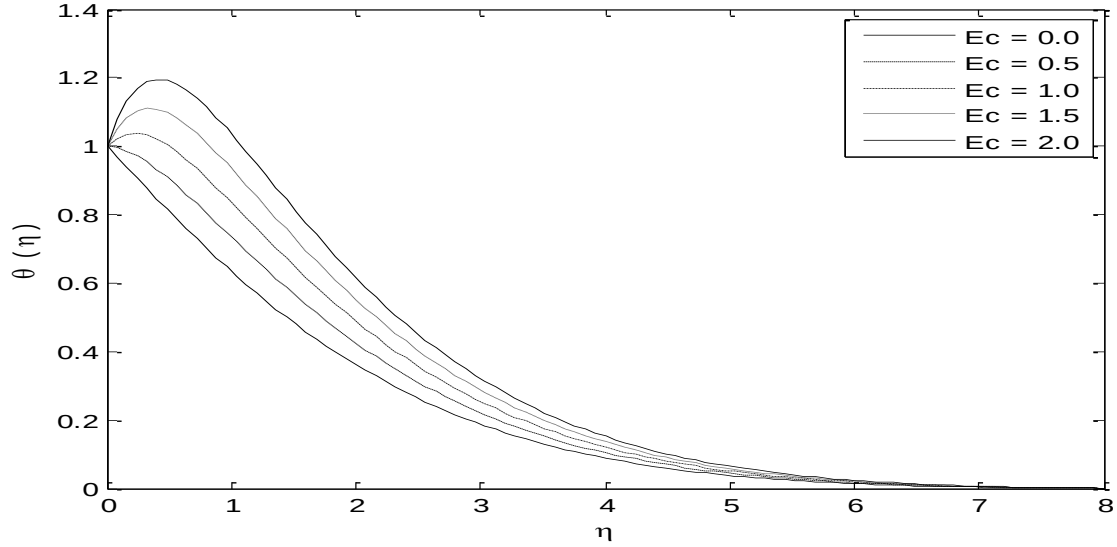

Figure 14. $\theta(\eta)$ **for** $n = 0.2, We = 0.2, Aa = 0.2, \gamma = 0.5,\ Sc = 0.5, Pr = 0.4, M = 0.3$ **and various** $Rd.$

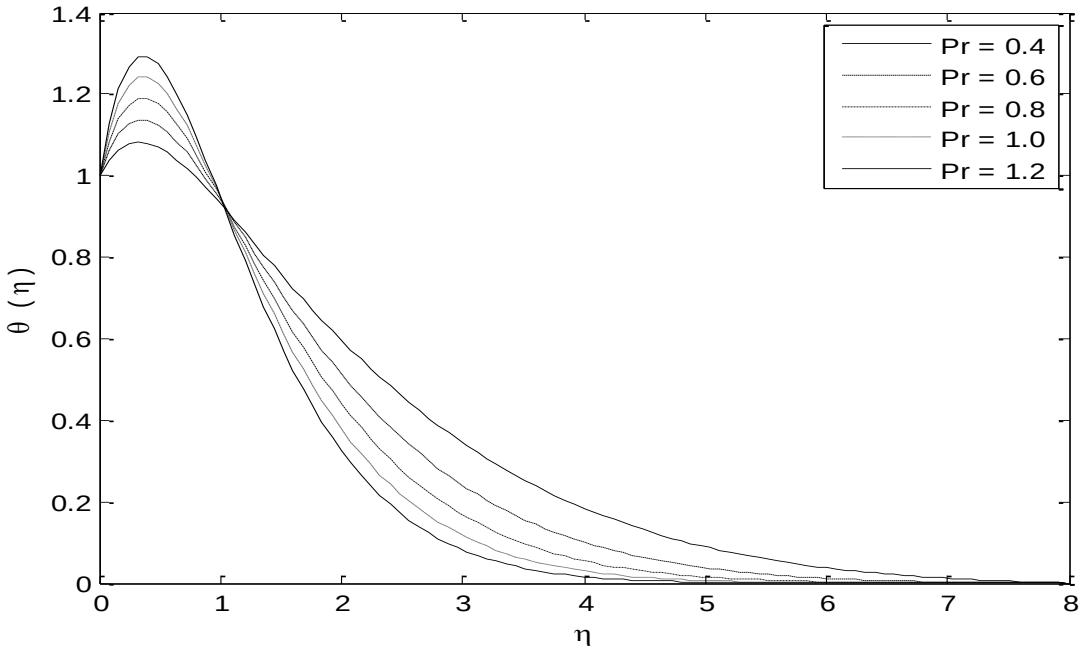

Figure 15. $\theta(\eta)$ **for** $n = 0.2, We = 0.2, Aa = 0.2, Ec = 1.0, Sc = 0.5, \gamma = 0.5, M = 0.5$ **and various** Pr

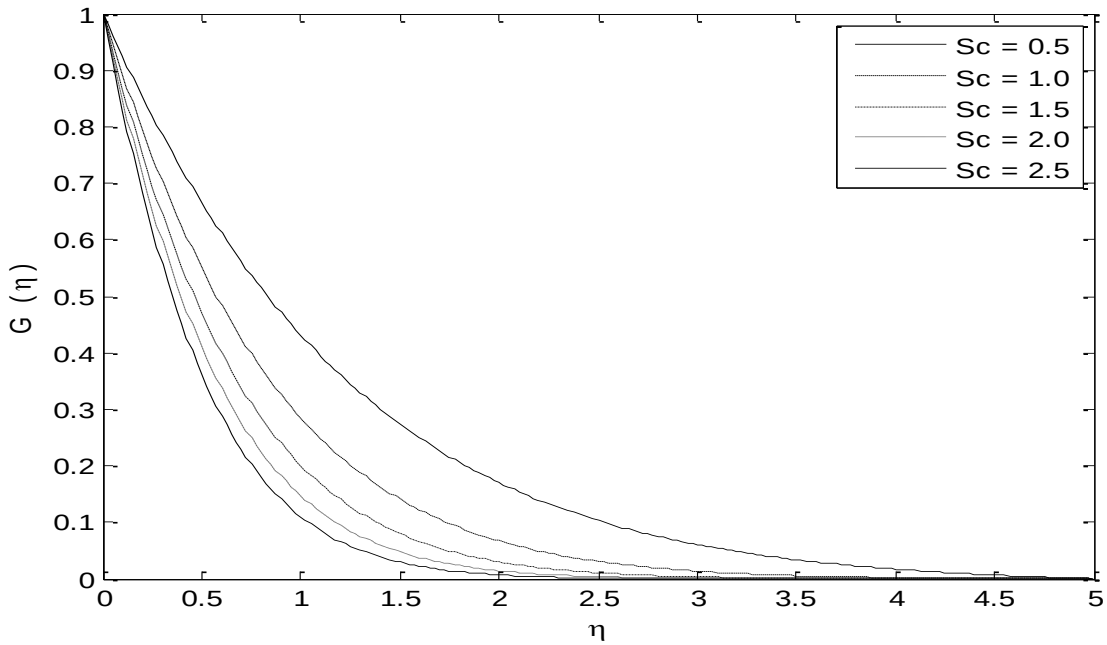

Figure 16. $G(\eta)$ **for** $n = 0.2, We = 0.2, Aa = 0.2, Ec = 0.5, Pr = 0.5, \gamma = 0.9, M = 1.0$ **and various** Sc**.**

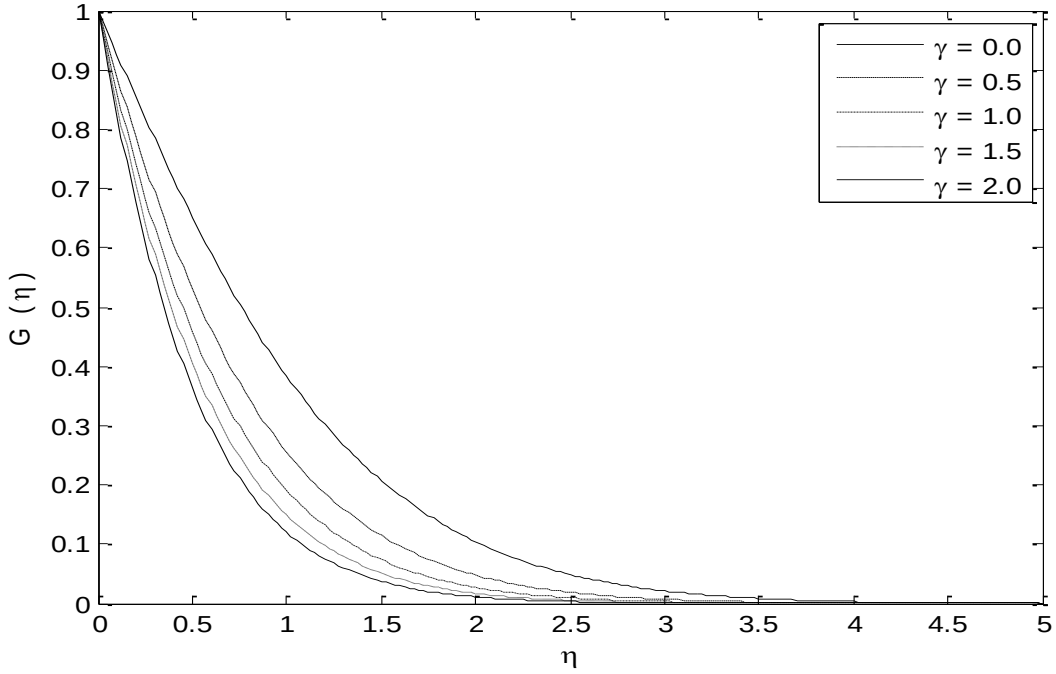

Figure 17. $G(\eta)$ **for** $n = 0.2, We = 0.2, Aa = 0.2, Ec = 0.5, Pr = 0.5, Sc = 1.5, M = 1.0$ **and various** γ.

Table 1. Comparison of numerical values of skin friction coefficient with Akber et al. [27] when $n = We = Aa = 0$.

M	Present Result	Akber et al. [27]
0.0	1	1
0.5	-1.11803	-1.11803
1	-1.41421	-1.41421
5	-2.44948	-2.44948

Table 2. Effect of the magnetic parameter M **on skin friction coefficient, local Nusselt and Sherwood number for** $n = 0.2, We = 0.2, Aa = 0.2, Ec = 0.5, Pr = 0.5, Sc = 1.5, \gamma = 0.9$

M	$\mathrm{Re}_x^{1/2} C_{f_x}$	$\mathrm{Re}_x^{-1/2} Nu_x$	$\mathrm{Re}_x^{-1/2} Sh_x$
0.0	-0.813259192023848	0.120183092238397	0.647833280722470
0.5	-0.952295767794350	-0.105694867310673	0.639909777779266
1.0	-1.073485498959232	-0.360094008439162	0.634108753717850
1.5	-1.182062692957529	-0.646731529489699	0.629431095705559
2.0	-1.281169050520400	-0.963511657004066	0.625570394955144

Table 3. Effect of the power law index n on skin friction coefficient, local Nusselt and Sherwood number for $We = 0.2, Aa = 0.1, Ec = 0.5, Pr = 0.5, Sc = 1.5, \gamma = 0.9, M = 0.5$.

n	$\mathrm{Re}_x^{1/2} C_{f_x}$	$\mathrm{Re}_x^{-1/2} Nu_x$	$\mathrm{Re}_x^{-1/2} Sh_x$
0.0	-1.076495078120168	0.085957850196534	0.646791697717219
0.1	-1.016609020792773	0.002337115841708	0.643342424149722
0.2	-0.952291322352062	-0.105698832531829	0.640029687250161
0.3	-0.882247758054356	-0.270531942274310	0.636030303173687
0.4	-0.804340715351971	-0.553030011464068	0.631267231004493

Table 4. Effect of the Weissenberg number We on skin friction coefficient, local Nusselt and Sherwood number for $n = 0.2, Aa = 0.2, Ec = 0.5, Pr = 0.5, Sc = 1.5, \gamma = 0.9, M = 0.8$.

We	$\mathrm{Re}_x^{1/2} C_{f_x}$	$-\mathrm{Re}_x^{-1/2} Nu_x$	$\mathrm{Re}_x^{-1/2} Sh_x$
0.0	-0.962754764878127	0.060240721716891	0.641231111403267
0.5	-0.935695564108154	0.172537533147468	0.638846967939806
1.0	-0.904610192735773	0.342922646700838	0.637020289387440
1.5	-0.867446847765413	0.709843966938974	0.634629531727002
2.0	-0.798628749344169	4.487088080101609	0.630935572091644

Table 5. Effect of the ratio of rates Aa on skin friction coefficient, local Nusselt and Sherwood number for $n = 0.2, We = 0.2, Ec = 0.3, Pr = 0.5, Sc = 1.5, \gamma = 0.9, M = 0.5$.

Aa	$\mathrm{Re}_x^{1/2} C_{f_x}$	$\mathrm{Re}_x^{-1/2} Nu_x$	$\mathrm{Re}_x^{-1/2} Sh_x$
0.8	-0.294696607913760	0.471699867776056	0.714469826887036
0.9	-0.151654757246047	0.529678756057184	0.726785500064597
1.0	-7.199034951957116e-08	0.561960901631355	0.739312177145388
1.1	0.160020333777360	0.564044381763420	0.751732658684006
1.2	0.328191783229816	0.530807496064778	0.764017487615885

Table 6. Effect of the Eckert number Ec on local Nusselt for $n = 0.2$, $We = 0.2, Aa = 0.2, \gamma = 0.9, Pr = 0.5, Sc = 1.5, M = 1.0$.

Ec	$\mathrm{Re}_x^{-1/2} Nu_x$
0.0	0.408237478632891
0.5	-0.105318796879050
1.0	-0.613524905212834
1.5	-1.121426253712503
2.0	-1.629310138259132

Table 7. Effect of the Prandtl number Pr on local Nusselt for $n = 0.2$, $We = 0.2, Aa = 0.2, Ec = 0.3, Sc = 1.5, \gamma = 0.9, M = 0.5$.

Pr	$-\mathrm{Re}_x^{-1/2} Nu_x$
0.4	0.034060425649880
0.6	0.169613404403348
0.8	0.280848749712570
1.0	0.391069710393603
1.2	0.501195481986016

Table 8. Effect of the Schmidt number Sc on Sherwood number for $n = 0.2$, $We = 0.2, Aa = 0.2, Ec = 0.3, Pr = 0.5, \gamma = 0.9, M = 1.0$.

Sc	$\mathrm{Re}_x^{-1/2} Sh_x$
0.5	0.640617318299022
1.0	0.925450626723974
1.5	1.021485454856626
2.0	1.345696150156854
2.5	1.516928451720601

Table 9. Effect of the chemical reaction parameter γ on Sherwood number for $n = 0.2, We = 0.2, Aa = 0.2, Ec = 0.3, Pr = 0.5, Sc = 1.5, M = 1.0$

γ	$\mathrm{Re}_x^{-1/2} Sh_x$
0.0	0.408237478633078
0.5	0.637179068821512
1.0	0.813575390218766
1.5	0.957759647549175
2.0	1.082455698542342

The consequence of the magnetic parameter on streamwise velocity $\mathrm{F}'(\eta)$ is shown in Fig. 1 Since M is the quotient of electromagnetic force to the inertial force, so by increasing M the Lorentz force increases which resists the fluid motion thus velocity profile and the associated momentum boundary layer thickness both decreases with the increasing value of M. In Fig. 2, normal velocity profile $\mathrm{F}(\eta)$ decreases with the increase in the magnetic parameter M. Fig. 3 shows the increasing trend of temperature profile $\theta(\eta)$ and thermal boundary layer for larger value of M because when magnetic parameter's value upsurges, the velocity of the fluid particle decreases thus more heat is absorbed by the fluid particles and hence the temperature profile of the fluid rises. Fig. 4 reveals the behavior of concentration profile $G(\eta)$ for different values of the magnetic parameter M. Figures. 5 & 6 demonstrate that both the streamwise velocity $\mathrm{F}'(\eta)$ and normal velocity $\mathrm{F}(\eta)$ profile decreases by increasing n, besides the momentum boundary layer thickness reduces in Fig. 5. Fig. 7

displays an increment in temperature profile $\theta(\eta)$ for different values of power law index n. Consequently, thermal boundary layer also increases here. The impact of the Weissenberg number We on velocity profile is explained in Figures. 8 & 9. Weissenberg number is a ratio of relaxation time to the specific process time, it increases the fluid thickness thus streamwise velocity profile $\mathrm{F}'(\eta)$ declines for larger values of We. Moreover, the associated momentum boundary layer in Fig. 8 reduces for higher value of We. Same trend is observed for normal velocity profile $\mathrm{F}(\eta)$ in Fig. 9. Fig. 10 shows the increasing trend of thermal boundary layer for increasing values of We.

The effect of the ratio of rates parameter Aa on streamwise velocity profile $\mathrm{F}'(\eta)$ is explored in Fig. 11. It is noticed that for greater values of the parameter Aa, the velocity profile increases. The associated boundary layer thickness has different effect for different values of Aa. For $Aa < 1$, the boundary layer thickness decrease and increases for $Aa > 1$. For $Aa = 1$, there is no boundary layer because surface and fluid travels with the identical velocities. In Fig. 12 normal velocity profile $\mathrm{F}(\eta)$ increases with increase in Aa. Fig. 13 explores that the temperature profile has a reducing effect for higher values of Aa. The characteristic of the Eckert number Ec on the temperature distribution $\theta(\eta)$ is plotted in Fig. 14. It is noticed that increase in temperature profile $\theta(\eta)$ and the boundary layer thickness is observed when the Eckert number Ec increases. Fig. 15 explains the behavior of the Prandtl number Pr on temperature profile $\theta(\eta)$. It illustrates that for higher values of Pr temperature profile $\theta(\eta)$ and thermal boundary layer increases in the narrow region in the neighborhood of the sheet but decreases away from the sheet. Fig. 16 depicts the concentration profile $G(\eta)$ for varying values of the Schmidt number Sc. It shows a decrement in concentration profile for larger values of Sc. Fig. 17 provides the investigation for variation of the chemical reaction parameter γ on $G(\eta)$. It detects that concentration profile $G(\eta)$ descends with the rise of γ.

In order to validate the accuracy of the method used, comparison of Skin friction coeffiecient for various values of M in the absence of n, Aa and We is shown in Table 1 which shows the excellent agreement with previous published results [27]. Table 2 represents the behavior of the magnetic parameter M on skin friction coefficient, local Nusselt number and Sherwood number for fixed values of the power law index n, the Weissenberg number, the Eckert number, the chemical reaction parameter, the Schmidt number and the Prandtl number. It shows that with the increase of the magnetic parameter M, the skin friction coefficient and local Nusselt number increases whereas local Sherwood number decreases. Table 3 shows decrease in skin friction coefficient and Sherwood numbers, while increase in local Nusselt with the increment of the power law index n. Table 4 shows the effect of Weissenberg number. Which shows the decreasing behavior of skin friction coefficient and Sherwood whereas increasing behavior of Nusselt number for varying values of We. The effect of the ratio of rates parameter Aa is described in Table 5 which depicts that Nusselt and Sherwood numbers increases gradually for larger value of Aa and skin friction coefficient has different impact on Aa. Effect of Eckert number on Nusselt number is depicted in Table 6, which exhibits increment in Nusselt number for higher value of Ec. Similarly the impact of the Prandtl number shows the enhancing behavior of Nusselt number for higher value of Pr in Table 7. In Tables 8 and 9, the influence of Schmidt number Sc and the chemical reaction parameter γ show the increasing trend of Sherwood number.

4. CONCLUSIONS

A numerical study of a Magnetohydrodynamic stagnation point flow of a tangent hyperbolic fluid with viscous dissipation is examined. The consequent facts are worth stating. The velocity profiles (both the streamwise and normal) declines for higher values of the magnetic parameter M and power-law index n. A large value of Weissenberg number We effects in a reduction in streamwise as well as normal velocity. Temperature profile increases for higher value of magnetic parameter M, the power-law index n and Weissenberg number We and decreases for larger values of the ratio of rates parameter Aa. A higher value of the Eckert number Ec results in an increase of temperature distribution. The behavior of streamwise velocity is different for Aa<1 and Aa>1. The Sherwood number and local Nusselt number decrease for higher values of magnetic parameter M. The local Nusselt number increases for larger values of the Eckert number and the Prandtl number. The Sherwood number demonstrates the increasing trend for greater values of the Schmidt number and the chemical reaction parameter.

REFERENCES

[1] Basha, P.M.S., Krishna M.V., Nagarathna N., *Heat Transfer*, **49**, 4264, 2020.
[2] Khan, W.A., Pop, I., *International Journal of Heat and Mass Transfer*, **53**, 2477, 2010.
[3] Nazar, M., Amin, N., Pop, I., *Mechanics Research Communication*, **31**, 121, 2004.
[4] Wang, C.Y., *Real World Applications*, **10**, 375, 2009.
[5] Rana, P., Bhargava, R., *Communications in Nonlinear Science and Numerical Simulation*, **17,** 212, 2012.
[6] Khan, J.A., Mustafa, M., Hayat, T., Alsaedi, A., *Plos One*, **10**(9), e0137363, 2015.
[7] Cortell, R., *Physics Letter A*, **372,** 631, 2008.
[8] Pramanik, S., *Ain Shams Engineering Journal*, **5**, 205, 2014.
[9] Ashraf, M., Ashraf, M.M., *Applied Mathematics and Mechanics*, **32**, 45, 2011.
[10] Shah, S., Hussain, S., Sagheer, M., *Results in Physics*, **9**, 303, 2018
[11] Mustafa, M., Hayat, T., Pop, I., Asghar, S., Obaidat, S., *International Journal of Heat and Mass Transfer*, **54**, 5588, 2011.
[12] Lok, Y.Y., Merkin, J.H., Pop, I, *Journal of Fluid Mechanics*, **812**, 418, 2017
[13] Khan, I., Ullah, S., Malik, M.Y., Hussain, A., *Results in Physics*, **9** 1141, 2018.
[14] Ashraf, M., Batool, K., *Journal of Theoretical and Applied Mechanics*, **51**, 25, 2013.
[15] Mohyud-Din, S.T., Khan, U., Ahmed, N., Rashidi, M.M., *Propulsion and Power Research*, **7**, 72, 2018.
[16] Sulochana, C., Samrat, S.P. Sandeep, N., *Propusion and Power Research*, **7**, 91, 2018
[17] Turkyilmazoglu, M., *Journal of Heat Transfer*, **134**, 071701, 2012.
[18] Sandeep, N., Sulochana, C., Kumar, B.R., *Engineering Science and Technology, an International Journal*, **19**, 227, 2016.
[19] Baag, S., Mishra, S.R., Dash, G.C., Acharya, M.R., *Ain Shams Engineering Journal*, **8**, 623, 2017.
[20] Hayat, T., Shehzad, S.A., Qasim, M., Obaidat, S., *Nuclear Engineering and Design*, **243,** 15, 2012.
[21] Turkyilmazoglu, M., Naganthran, K., Pop, I., *International Journal of Numerical Methods for Heat & Fluid Flow*, **27**, 1554, 2017.

[22] Kumar, K., Gireesha, B.J., Krishanamurthy, M.R., Rudraswamy, N.G., *Results in Physics*, **7**, 3031, 2017.
[23] Nadeem, S., Akram, S., *Acta Mechanica Sinica*, **27**, 237, 2011.
[24] Nadeem, S., Shahzadi, I., *AIP advances*, **6**, 015110, 2016.
[25] Akbar, N.S., Nadeem, S., Ul Haq, R., Khan, Z.H., *Indian Journal of Physics*, **87**, 1121, 2013.
[26] Iqbal, Z., Azhar, E., Maraj, E.N., Ahmad, B., *Frontiers in Heat and Mass Transfer*, **8**, 25, 2017.
[27] Akbar, N.S., Nadeem, S., Hayat, T., Hendi, A.A., *International Journal of Heat and Mass Transfer*, **54**, 4360, 2011.
[28] Hayat, T., Riaz, A., Tanveer, A., Alsaedi, A., *Thermal Science and Engineering Progress*, **6**, 217, 2018.
[29] Abbasi, M.A., Bai, Y.Q., Bhatti, M.M., Rashidi, M.M., *Alexandria Engineering Journal*, **55**, 653, 2016.
[30] Salahuddin, T., Malik, M.Y., Hussain, A., Awais, M., Khan, I., Khan, M., *Results in Physics*, **7**, 426, 2017.
[31] Hayat, T., Qayyum, S., Ahmad, B., Waqas, M., *The European Physical Journal Plus*, **131**, 422, 2016.
[32] Khan, M.I., Hayat, T., Alsaedi, A., Khan, M. I., *International Journal of Heat and Mass Transfer*, **113,** 310, 2017.
[33] Motsumi, T.G., Makinde, O.D., *Physica Scripta*, **86**, 045003, 2012.
[34] Bataller, R.F., *International Journal of Heat and Mass Transfer*, **50**, 3152, 2007.
[35] Anantha Kumar K., Sugunamma, V., Sandeep, N., *J Therm Anal Calorim* **139,** 3661, 2020.
[36] Turkyilmazoglu, M, *Archives Of Mechanics*, **71**, 49, 2019.
[37] Khan, M., Rasheed, A., Salahuddin, T., *AIP Advances*, **10**, 075211, 2020.